www.springer.com/41230
https://doi.org/10.1007/s41230-026-5268-1
Research & Development
Vol. 23 No. 4 July 2026
CHINA FOUNDRY

Formation mechanism of film-like spinel inclusions in Ni-based superalloys from MgO crucible reaction

***Wen-jin Wu[1], Feng-wei Guo[1], Wei-jie Xing[1], Li-hui Zhang[1], Min Xia[2], Xiao-dong Ren[1], and Lei Qian[1]**

1. Science and Technology on Advanced High Temperature Structural Materials Laboratory, Beijing Institute of Aeronautical Materials, Beijing 100095, China

2. Institute of Powder Metallurgy and Advanced Ceramics, University of Science and Technology Beijing, Beijing 100083, China

Abstract: Film-like $MgAl_2O_4$ spinel inclusions are among the most harmful oxide defects in Ni-based superalloys because their high aspect ratio exacerbates local stress concentration. In this work, K492M Ni-based superalloy was remelted and cast in a MgO-containing crucible using a vacuum induction furnace to clarify the origin and formation pathway of Mg-, Al-, and O-bearing inclusions. Scanning electron microscopy, transmission electron microscopy, energy-dispersive spectroscopy, and selected-area electron diffraction were used to characterize the morphology, composition, and crystal structure of the inclusions. The results show that the inclusions consist mainly of particulate MgO cores directly coated by $MgAl_2O_4$ shells, together with flocculent film-like $MgAl_2O_4$ products extending outward from the cores. Only local residual α-Al_2O_3 is detected, indicating that Al_2O_3 is a transient intermediate rather than a stable final product. Based on these observations, a three-stage mechanism is proposed: mechanical spallation of MgO particles from the crucible wall, rapid interfacial reduction coupled with solid-state transformation to form $MgAl_2O_4$, and stress-induced rupture and exfoliation of the spinel shell into thin films. This mechanism explains the coexistence of MgO-$MgAl_2O_4$ core-shell particles and film-like spinel inclusions, and provides guidance for controlling crucible-derived oxide contamination in Ni-based superalloy castings.

Keywords: K492M alloy; Ni-based superalloy; vacuum induction remelting; MgO crucible; $MgAl_2O_4$ spinel; film-like inclusion; interfacial reaction

CLC numbers: TG146.1+5 **Document code:** A **Article ID:** 1672-6421(2026)04-591-08

1 Introduction

Nickel-based superalloys are widely used in hot-section components of aero-engines and gas turbines because of their excellent high-temperature strength, creep resistance, and corrosion resistance[1-4]. As engine operating temperatures and thrust-to-weight ratios continue to increase, alloy cleanliness has become a key requirement for service reliability[5-8]. Non-metallic inclusions formed during melting and casting can act as crack-initiation sites and reduce fatigue life[9-17]. Among these defects, oxide inclusions are particularly important because they are hard, brittle, and often weakly bonded to the Ni-based matrix[18-20].

The damage caused by oxide inclusions depends strongly on their size and morphology[15, 16]. Film-like oxides are especially detrimental because their high aspect ratio produces severe stress concentration[19, 20]. Accident investigations of turbine components have reported failures associated with large film-like MgO-Al_2O_3-TiN or Al-Mg-O inclusions in Ni-based superalloy rotors, highlighting the need to understand both the source and morphological evolution of such inclusions.

Vacuum induction melting (VIM) and vacuum induction remelting (VIR) are commonly used to produce superalloy master alloys and castings. These processes promote degassing and compositional control under low oxygen potential[21-24]. However,

***Wen-jin Wu**

Engineer, specializing in cast equiaxed superalloys and engineering-scale research. His work focuses on casting process development and alloy performance optimization.

E-mail: brent_Woo@163.com

Received: 2025-11-01; Revised: 2026-02-05; Accepted: 2026-02-28

reactions between reactive alloying elements and refractory crucible materials can introduce oxide inclusions and therefore limit melt cleanliness[7, 25, 26].

Crucible-derived inclusions are governed by both physical and chemical processes. Melt convection and thermal shock can detach refractory particles from the crucible lining, while dissolved reactive elements such as Al and Ti can react with these particles after they enter the melt[27, 28]. Studies on molten steel-refractory systems provide a useful reference for understanding refractory reduction and oxide transformation[29-32], but Ni-based superalloys contain higher levels of reactive alloying elements. Therefore, the reaction products and inclusion morphologies in superalloy melts can differ markedly from those in steel systems.

Previous studies on high-Al and high-Ti Ni-based superalloys have shown that MgO crucibles can react with dissolved Al to form Mg- and Al-containing oxides[33, 34]. The commonly accepted model describes a stepwise pathway: MgO is first reduced by Al to form Al_2O_3, and the newly formed Al_2O_3 subsequently reacts with MgO to produce a $MgAl_2O_4$ spinel layer[28]. In most reports, this spinel layer is regarded as the final product, and the inclusions are described mainly as fine particles or continuous interfacial coatings[17, 18]. However, this model does not fully explain how detached MgO particles evolve into film-like spinel inclusions, nor why independent Al_2O_3 is rarely observed in many MgO-$MgAl_2O_4$ core-shell structures.

To address this problem, the present work investigated Mg-containing inclusions in K492M Ni-based superalloy produced by vacuum induction remelting and casting in a MgO crucible. SEM, FIB, TEM, EDS, and SAED analyses were combined with thermodynamic and kinetic considerations to clarify the inclusion source, phase relationship, and morphological evolution. A dynamic mechanism involving mechanical spallation, coupled reduction/phase transformation, and stress-induced film formation was proposed to explain the formation of film-like $MgAl_2O_4$ inclusions.

2 Experiment

2.1 Experimental materials

The material used in this study was K492M Ni-based superalloy. Its chemical composition was determined by inductively coupled plasma spectrometry (ICP) and glow discharge mass spectrometry (GDMS), as listed in Table 1.

Table 1: Chemical composition of K492M alloy (wt.%)

Cr	Mo	W	Al	Ta	Ti	Co	C	B	Zr	O (ppm)	Mg (ppm)	Ni
12.5	1.9	4.1	3.4	4.2	4.1	9.1	0.08	0.01	0.02	8	15	Bal.

2.2 Experimental procedure

Melting and pouring experiments were conducted in a vacuum induction furnace. The vacuum system consisted of a mechanical pump, a Roots pump, and an oil booster pump, with an ultimate vacuum of 10^{-2} Pa and a leakage rate of $\leq$0.5 Pa·min^{-1}. An MA-14 crucible, mainly composed of 87.35vol.% MgO and 12.65vol.% MgO-Al_2O_3, was used. For each experiment, 3 kg of K492M master alloy was charged into the crucible. The alloy was remelted by gradually increasing the power to reach 1,570 °C, and then held for 10 min to ensure homogenization. Subsequently, the molten alloy was poured into a ceramic mold to obtain a casting ingot with a diameter of 90 mm and a height of 65 mm.

2.3 Characterization methods for oxide inclusions

After cooling to room temperature, the ingot was sectioned into 8 mm-thick slices. Inclusions on these slices were first located by fluorescent penetrant inspection. Specimens containing inclusion defects were then extracted by precision wheel cutting and electrical discharge machining.

The morphology and composition of the oxide inclusions were characterized using a field-emission scanning electron microscope (FESEM, Crossbeam 550, Carl Zeiss AG, Germany) equipped with an energy-dispersive X-ray spectrometer (EDS, Ultim Max 65, Oxford Instruments, UK). Focused ion beam (FIB) milling was then performed using a HELIOS NanoLab 600I dual-beam microscope to prepare site-specific thin foils. The foils were thinned to a thickness of approximately 80–100 nm for transmission electron microscopy (TEM) observation. Microstructural and phase analyses were conducted on a Tecnai G2 transmission electron microscope operated at 200 kV using TEM and high-resolution TEM (HRTEM).

3 Results

3.1 Morphology and composition of inclusions

SEM observations reveal composite oxide inclusions dispersed in the matrix. As shown in Figs. 1 and 2, these inclusions contain one or more particulate cores and film-like products extending from their peripheries. Figure 1 shows a typical irregular particulate inclusion core with a size of approximately 100 μm in the secondary-electron image. Its morphology is similar to the granular refractory material in the crucible. EDS mapping shows that the core is enriched in Mg and O, confirming that it is MgO. A continuous peripheral layer enriched in Mg, Al, and O is tightly attached to the MgO core, indicating the formation of an interfacial reaction product rather than pure MgO.

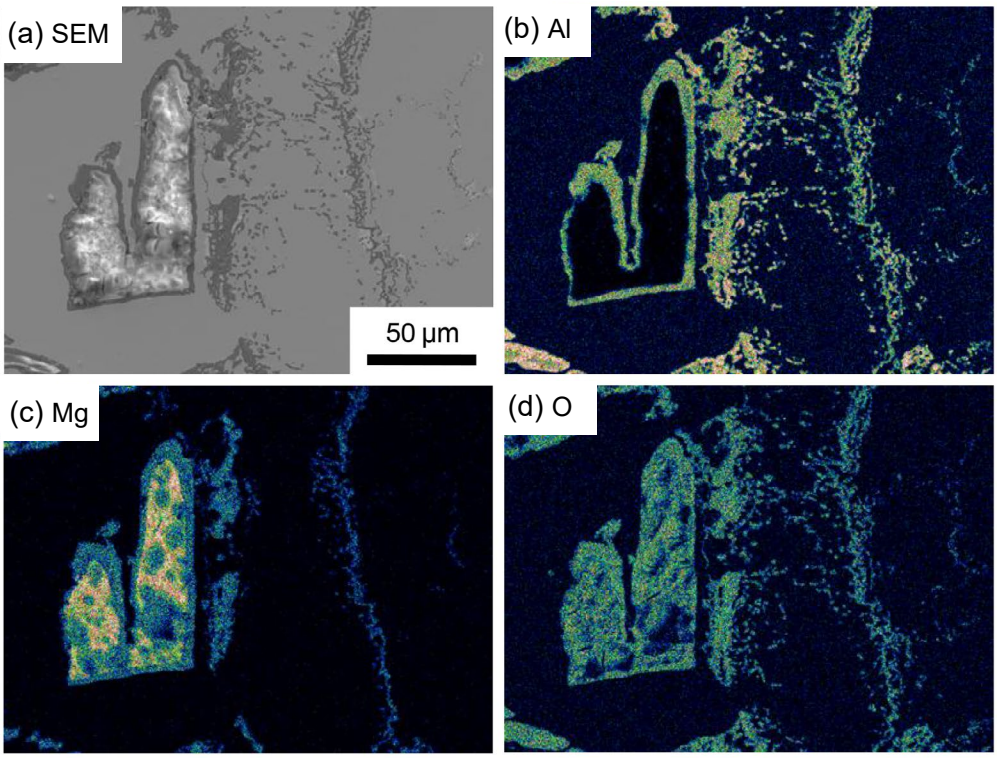

Fig. 1: Macroscopic distribution of inclusions in K492M alloy (a) and the corresponding EDS elemental mapping results (b–d)

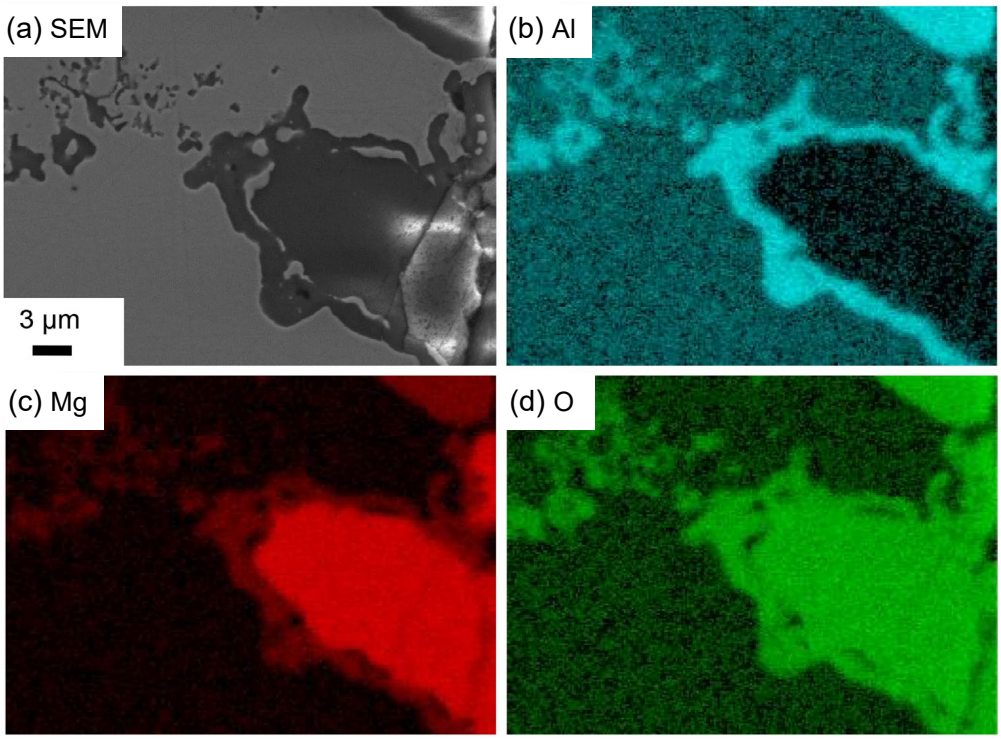

Fig. 2: Magnified view of a typical inclusion region showing its detailed microstructure (a), and the corresponding EDS elemental mapping results (b–d)

Flocculent or vein-like films are frequently observed around the MgO-cored particles (Fig. 2). These films extend from the particle edges and appear as torn or flocculent features in two-dimensional SEM projection. EDS mapping confirms that the films are uniformly composed of Mg, Al, and O, consistent with the coating layer on the particulate core. The coexistence of a particulate core and emanating films indicates an outward morphological evolution from the MgO particle.

3.2 Phase composition and crystalline structure of inclusions

To identify the crystalline phases and their relationships, site-specific samples from the inclusions described in Section 3.1 were prepared by FIB and analyzed by TEM.

Figure 3 shows the FIB lift-out regions and corresponding analytical targets. Two representative regions were selected:

Location 1 contains a particulate core and its surface film-like coating, whereas Location 2 contains an independent film-like oxide located in the matrix away from any particulate core.

Figure 4 shows the TEM high-angle annular dark-field (HAADF) image and EDS elemental analysis of Location 1 in Fig. 3. Selected-area electron diffraction (SAED) was performed on the particle core (Region A) and the surface coating (Region B). Region A is identified as periclase (MgO), whereas Region B is identified as magnesium aluminate spinel ($MgAl_2O_4$). These results provide crystallographic evidence that MgO particles are directly coated by $MgAl_2O_4$ films.

Figure 5 shows the HAADF image and the corresponding EDS elemental mapping of Location 2 in Fig. 3. The HAADF image clearly reveals the typical morphology of this independent film-like feature. Under HAADF conditions, the film exhibits light gray contrast against the dark gray matrix.

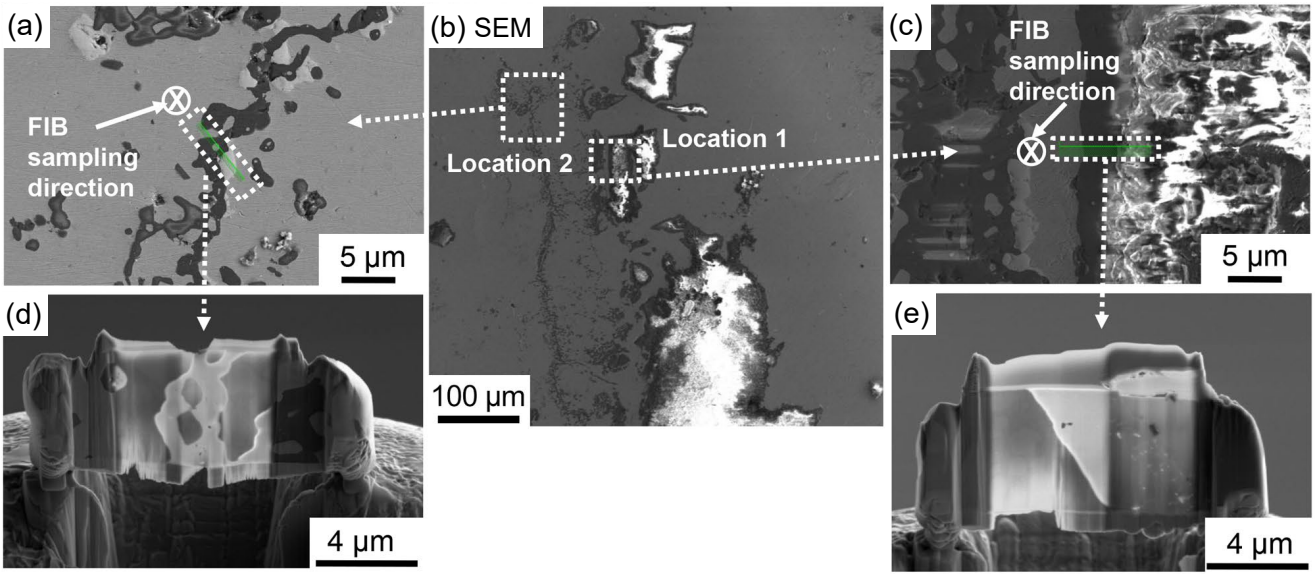

Fig. 3: Schematic diagram of inclusion sampling locations in K492M: (a, c) high-magnification SEM image of FIB sampling area at Locations 1 and 2 in (b); (b) overall SEM morphology of sample; (d, e) cross-sectional morphology of Locations 1 and 2 prepared by FIB sampling

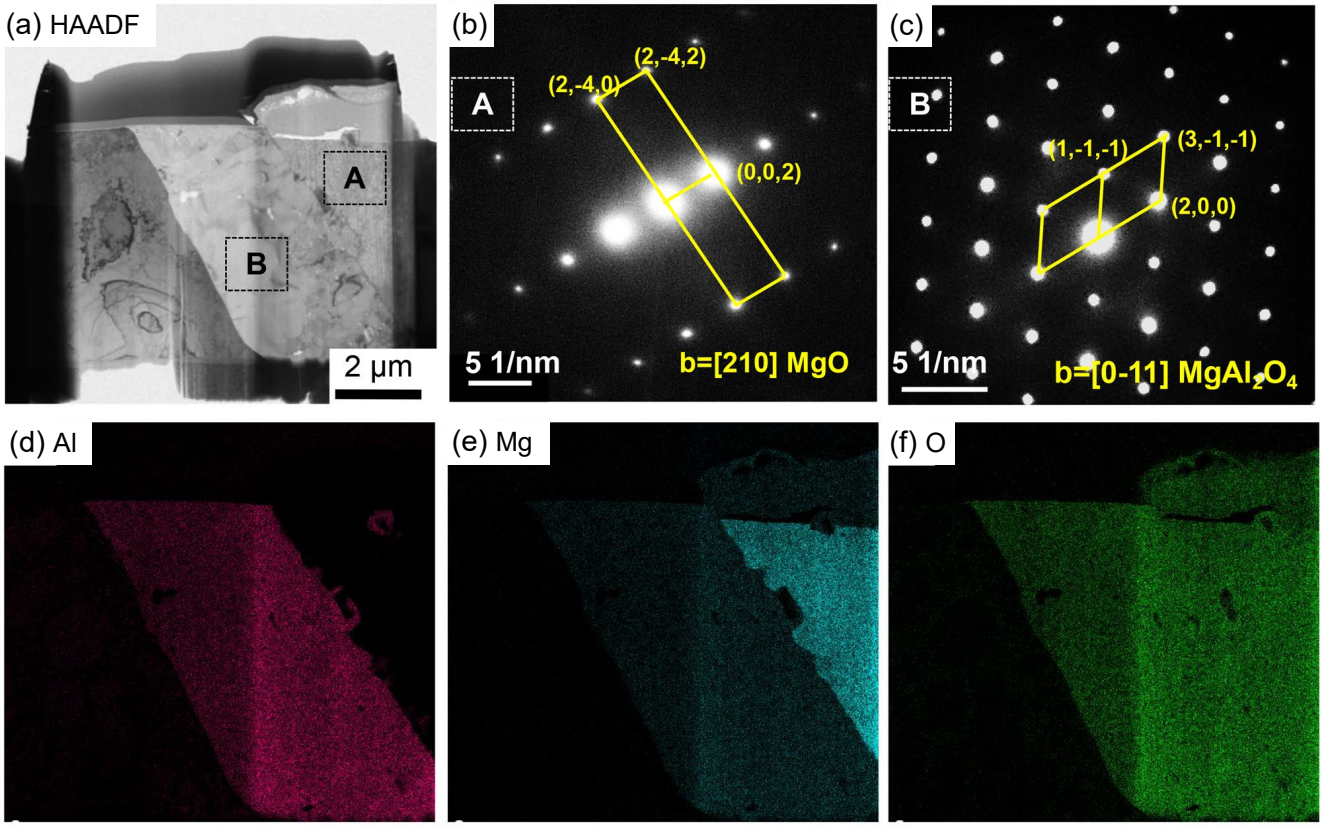

Fig. 4: HAADF image of a representative region (Location 1 in Fig. 3) (a), corresponding SAED patterns (b, c), and EDS elemental mapping results (d–f)

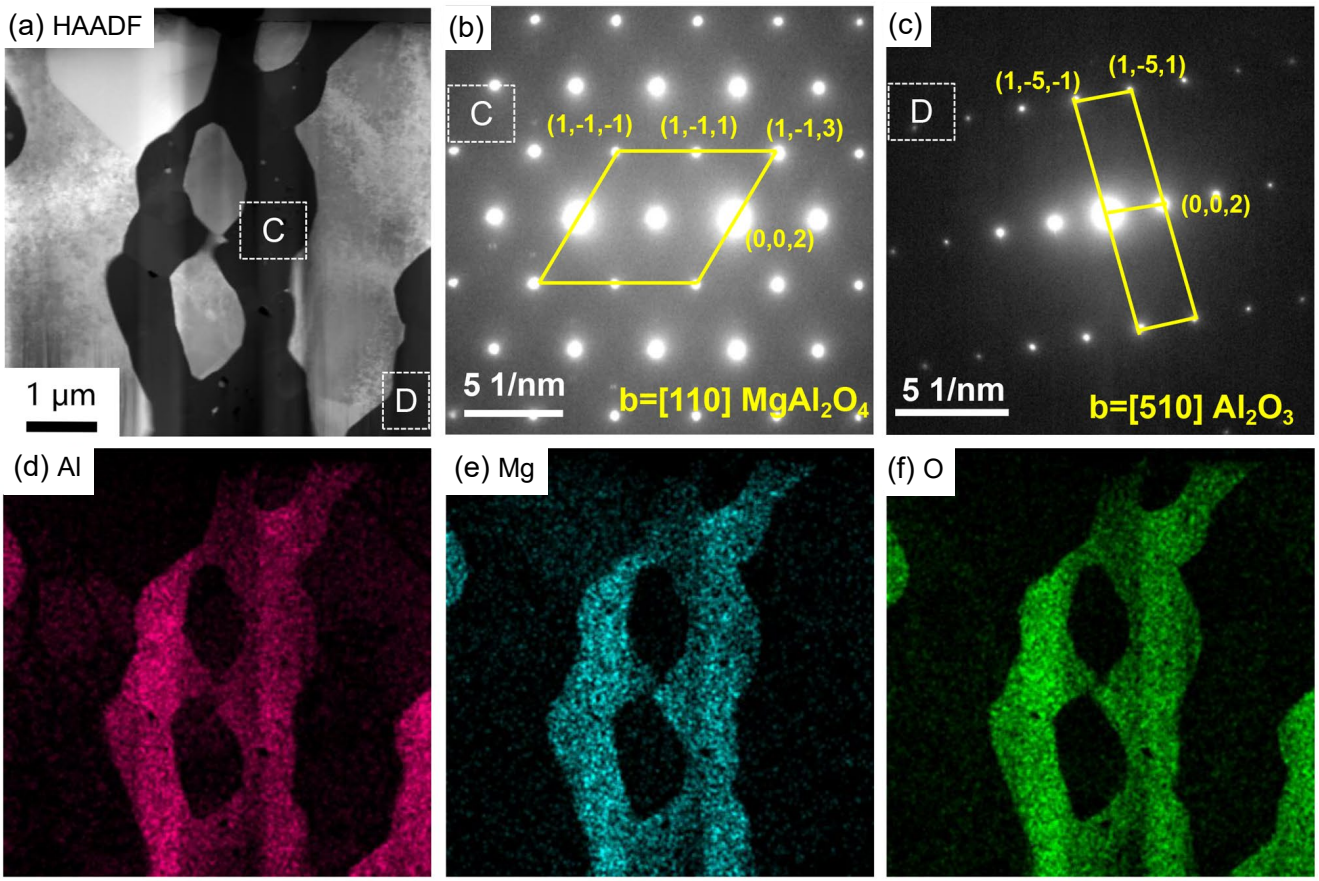

Fig. 5: HAADF image of a representative region (Location 2 in Fig. 3) (a), corresponding SAED patterns (b, c), and EDS elemental mapping results (d–f)

EDS mapping confirms that the film is uniformly composed of Mg, Al, and O. To further identify the phase, SAED analysis was performed separately on the film (Region C) and on a minute particle adjacent to the film edge (Region D). SAED analysis indicates that Region C (the film) is single-phase $MgAl_2O_4$, while Region D (a tiny particle near the film edge) is indexed as α-Al_2O_3.

These micro-area observations establish the phase relationships among the inclusion components. The particulate cores are MgO, both the coating layers and the independent films are $MgAl_2O_4$, and residual α-Al_2O_3 occurs only locally. The coexistence of MgO, α-Al_2O_3, and $MgAl_2O_4$ provides the experimental basis for analyzing the dynamic formation sequence of film-like spinel inclusions.

4 Discussion

The particulate MgO cores match the size and morphology of the crucible raw material, confirming their crucible origin. TEM micro-area analysis reveals that while a transient intermediate Al_2O_3 film coating the MgO particles is rarely captured, the prevalent observation is a $MgAl_2O_4$ film directly coating the MgO, from which typical film-like spinel emanates outward. This critical evidence indicates an extremely rapid transformation from MgO to $MgAl_2O_4$ and a very narrow "window" of stability for the independent Al_2O_3 intermediate phase.

Based on the aforementioned phenomena, the formation of film-like $MgAl_2O_4$ inclusions is described by a three-stage mechanism (Fig. 6): mechanical spallation of MgO particles, coupled interfacial reduction/solid-state phase transformation, and stress-induced rupture and film formation.

Stage I: Mechanical spallation of MgO particles

Mechanical spallation of MgO particles from the crucible wall provides the solid reactants for subsequent reactions. Under thermal stress, melt scouring, and vacuum melting conditions, microscopic MgO particles can detach from the crucible working lining and subsequently migrate into the alloy melt as highly active and dispersed solid reactants. Rather than a random incidental phenomenon, such spallation constitutes a probable physical behavior under the present manufacturing parameters and provides critical substrates for subsequent interfacial reactions in the molten alloy.

Stage II: Interfacial reaction and rapid solid-state phase transformation: direct formation of $MgAl_2O_4$ film

TEM observations show that spalled MgO particles are commonly encapsulated directly by $MgAl_2O_4$ films, whereas independent Al_2O_3 films are rare. Therefore, the traditional stepwise model, in which Al_2O_3 first forms and then reacts with MgO to form $MgAl_2O_4$ (Fig. 7), is better described in the present high-temperature melt as a rapid coupled process. First, dissolved [Al] reduces MgO at the interface. Then, the nascent Al_2O_3 immediately reacts with adjacent MgO through solid-state transformation. As shown in Fig. 8, these two steps

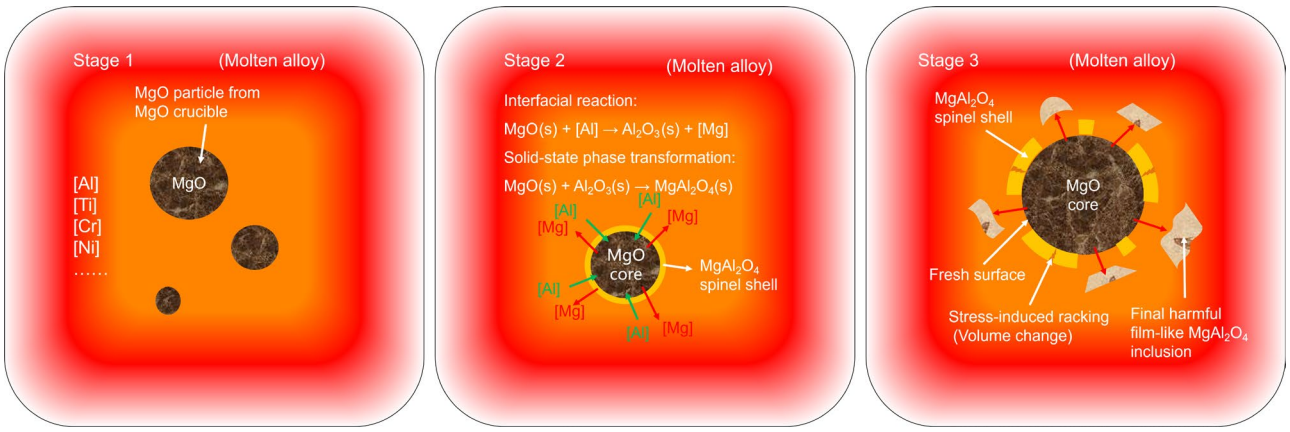

Fig. 6: Schematic diagram illustrating "three-stage" formation of inclusions

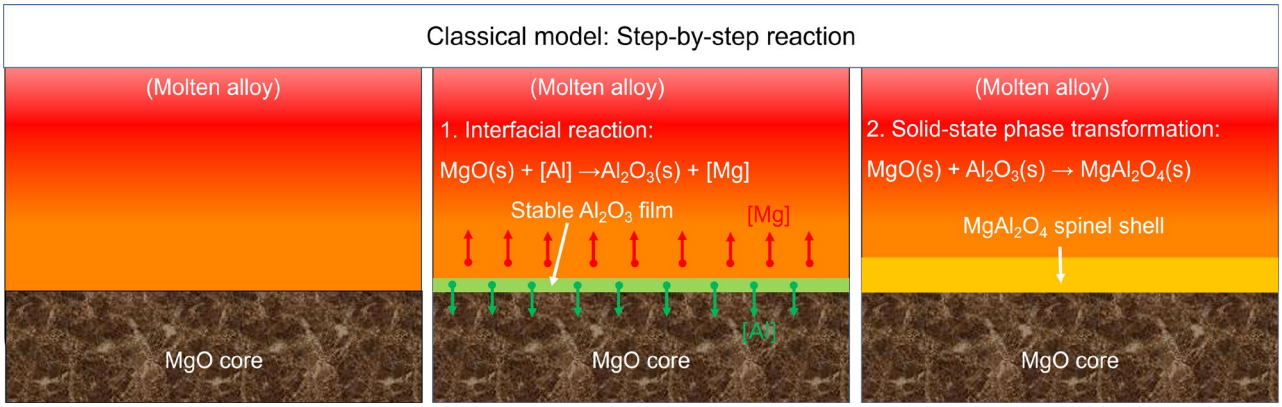

Fig. 7: Schematic illustration of traditional reaction model

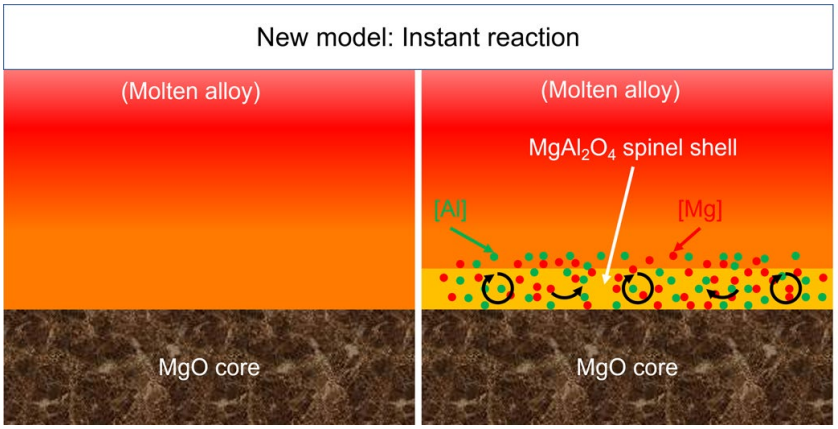

Fig. 8: Schematic illustration of new reaction model

are coupled and form a $MgAl_2O_4$ shell directly around the MgO core.

In contrast with the classical stepwise model[33], the interfacial reduction reaction between dissolved [Al] and MgO particles is the starting point of the process. Thermodynamically, Reaction (1) is favorable and can supply dissolved Mg and oxygen-containing reaction products in the melt:

$$3MgO(s) + 2[Al] \rightarrow Al_2O_3(s) + 3[Mg] \quad (1)$$

The key aspect of the new model is that the nascent Al_2O_3 is formed on the MgO surface via the aforementioned reduction reaction, it does not stably accumulate into a continuous and independent film. Due to the immediate presence of the MgO reactant substrate and the extremely high temperature (>1,500 °C), the ion diffusion rate at the interface is very rapid. Consequently, the nascent Al_2O_3 instantaneously undergoes a solid-state phase transformation with adjacent MgO:

$$MgO(s) + Al_2O_3(s) \rightarrow MgAl_2O_4(s) \quad (2)$$

Al_2O_3 exhibits an extremely short lifetime as a discrete phase for an exceptionally high rate in subsequent solid-state phase transformation. Therefore, TEM usually captures the post-reaction state: an $MgAl_2O_4$ film directly coating the MgO particle. The MgO-$MgAl_2O_4$ core-shell structure in Fig. 1 represents the final product of this coupled reduction and phase-transformation process. The local observation of α-Al_2O_3 in Fig. 5 may reflect rapid local cooling or incomplete transformation that temporarily preserves this intermediate phase.

Stage III: Solid-state phase transformation and the formation of film-like spinel inclusions

As the $MgAl_2O_4$ shell thickens, significant internal stress accumulates owing to volume variation during phase transformation. This stress can eventually induce shell rupture and exfoliation, followed by outward extension and dispersion, thereby forming an adverse film-like microstructure. SEM observations show that the exfoliated $MgAl_2O_4$ products generally appear as two-dimensional flocculent features. FIB cross-sectioning and TEM-HAADF analysis further confirm that these products are submicron-thick films rather than equiaxed particles.

The morphological evolution can therefore be described as follows: after stress-induced fracture of the $MgAl_2O_4$ shell, exfoliated fragments extend and tear within the high-temperature melt, ultimately forming initial ultrathin films. Melt convection then promotes plastic deformation, curling, and folding of these films before solidification. This process transforms dense MgO particles derived from the crucible into high-aspect-ratio flocculent $MgAl_2O_4$ films, which are more harmful than compact particles because they produce stronger stress concentration.

Overall, MgO crucible corrosion and spallation are the main sources of Mg-containing inclusions in the VIR K492M alloy. The proposed three-stage mechanism links refractory particle detachment, interfacial reaction, spinel transformation, and film formation, providing a mechanistic basis for suppressing crucible-derived spinel inclusions.

5 Conclusions

The formation mechanism of $MgAl_2O_4$ inclusions in K492M Ni-based superalloy during vacuum induction remelting was investigated using multi-scale microscopic characterization. The main conclusions are as follows:

(1) The Mg in Mg-Al-O composite inclusions originates mainly from the MgO crucible. The particulate MgO cores show size and morphological features consistent with the crucible raw material, providing direct evidence for crucible-derived contamination.

(2) The formation of $MgAl_2O_4$ inclusions follows a dynamic three-stage sequence: mechanical spallation, coupled interfacial reduction/solid-state phase transformation, and stress-induced film formation. The interfacial reaction between spalled MgO particles and dissolved [Al] is a rapid coupled process rather than a simple stepwise reaction. Nascent Al_2O_3 rapidly reacts with MgO to form a $MgAl_2O_4$ shell, leaving only a narrow time window for Al_2O_3 to exist as an independent phase.

(3) Effective control of film-like $MgAl_2O_4$ inclusions requires both suppression of crucible spallation/corrosion and interruption of the reaction pathway. Possible strategies include using more chemically stable crucible materials, shortening high-temperature holding time to reduce lining corrosion, and maintaining vacuum integrity to keep a low oxygen potential in the melt. These measures can improve melt cleanliness and casting reliability of Ni-based superalloys.

Acknowledgments

This research was financially supported by the National Key Research and Development Program of China (Grant No. 2022YFB3708100), the WDZC program of BIAM (Grant No. 2019-363), and the National Natural Science Foundation of China (Grant No. 52374360).

Conflict of interest

The authors declare that they have no conflict of interest.

References

[1] Reed R C. The superalloys: Fundamentals and applications. Cambridge: Cambridge University Press, 2006.
[2] Zhang J C, Lu F, Huang T W, et al. An advanced approach to improve the high-temperature property for Ni-based superalloys: Interface segregation manipulation. Materials Science and Engineering: A, 2023, 881: 145382.
[3] Huang J, Yan J, Lei D, et al. Tensile properties and deformation characteristics of nickel-iron-based superalloys for steam turbine rotors. Emergent Materials, 2024, 7(6): 3011–3028.
[4] Li G, Sun D, Guo L, et al. Microstructure evolution and tensile behavior of hot pressed powder metallurgy superalloys. Journal of Materials Research, 2023, 38(17): 4118–4129.
[5] Meetham G W. Trace elements in superalloys – An overview. Metals Technology, 2013, 11(1): 414–418.
[6] Holt R T, Wallace W. Impurities and trace elements in nickel-base superalloys. International Metals Reviews, 1976, 21(1): 1–24.
[7] Zhao Y, Wang L, Chen C, et al. Effect of a MgO-CaO-ZrO_2-based refractory on the cleanliness of a K4169 Ni-based superalloy. Ceramics International, 2023, 49(1): 117–125.
[8] Wang J, Wang L, Li J, et al. Effects of aluminum and titanium additions on the formation of nonmetallic inclusions in nickel-based superalloys. Journal of Alloys and Compounds, 2022, 906: 164281.
[9] Zhang T, Jiang J, Shollock B A, et al. Slip localization and fatigue crack nucleation near a non-metallic inclusion in polycrystalline nickel-based superalloy. Materials Science and Engineering: A, 2015, 641: 328–339.
[10] Stinville J C, Martin E, Karadge M, et al. Competing modes for crack initiation from non-metallic inclusions and intrinsic microstructural features during fatigue in a polycrystalline nickel-based superalloy. Metallurgical and Materials Transactions: A, 2018, 49: 3865–3873.
[11] Chan K S. A fatigue life model for predicting crack nucleation at inclusions in Ni-based superalloys. Metallurgical and Materials Transactions: A, 2020, 51(3): 1148–1162.
[12] Texier D, Stinville J C, Charpagne M A, et al. Role of non-metallic inclusions and twins on the variability in fatigue life in alloy 718 nickel base superalloy. In: Superalloys 2020: Proceedings of the 14th International Symposium on Superalloys, Cham: Springer International Publishing, 2020.
[13] Texier D, Stinville J C, Echlin M, et al. Short crack propagation from cracked non-metallic inclusions in a Ni-based polycrystalline superalloy. Acta Materialia, 2019, 165: 241–258.
[14] Stinville J C, Miller V M, Pollock T M. Effect of non-metallic ceramic inclusions on strain localization during low cycle fatigue of a polycrystalline superalloy. In: Superalloys 2016: Proceedings of the 13th International Symposium on Superalloys, Hoboken: John Wiley & Sons, 2016.

[15] Hu D, Wang T, Ma Q, et al. Effect of inclusions on low cycle fatigue lifetime in a powder metallurgy nickel-based superalloy FGH96. International Journal of Fatigue, 2018, 118: 237–248.
[16] Yao Z, Hou J, Chen Y, et al. Effect of micron-sized particles on the crack growth behavior of a Ni-based powder metallurgy superalloy. Materials Science and Engineering: A, 2022, 860: 144242.
[17] Bussac D A , Lautridou J. A probabilistic model for prediction of LCF surface crack initiation in PM alloys. Fatigue & Fracture of Engineering Materials & Structures, 1993, 16(8): 861–874.
[18] Gao X Y, Zhang L, Qu X H, et al. Investigation on the formation mechanism of non-metallic inclusions in high-aluminum and titanium-alloyed Ni-based superalloy. Vacuum, 2020, 177: 109409.
[19] Zhang L, Liu E, Xing W J, et al. The formation mechanism of oxide inclusions in a high-aluminum Ni-based superalloy during the vacuum induction remelting process. Metals, 2024, 14(6): 654.
[20] Liu E, Wu W, Fan W, et al. Role of aluminum and hafnium on the interfacial reactions between crucibles and nickel-based superalloys. Ceramics International, 2025, 51(24): 42815–42823.
[21] Yang Y, Wang Z, Zhang Y, et al. Deoxidation reaction during vacuum induction melting of solution superalloy. Journal of Iron and Steel Research, 2011.
[22] Niu J P, Sun X F, Jin T, et al. Deoxidation during vacuum induction melting of Ni-base superalloy. Chinese Journal of Nonferrous Metals, 2002, 12(2): 217–220. (In Chinese)
[23] Kennedy R L, Jones R F, Davis R M, et al. Superalloys made by conventional vacuum melting and a novel spray forming process. Vacuum, 1996, 47(6–8): 819–824.
[24] Li X Z, Feng H, Li H B, et al. Deoxidation of nickel-based superalloy using carbon under high vacuum degree. Metallurgical and Materials Transactions: B, 2024, 55(6): 4503–4517.
[25] Jeon J, Lindberg D. Interfacial reaction between different MgO-based refractories and the CaO-FeO_x-SiO_2 slag system at 1400 °C. Journal of the European Ceramic Society, 2025, 45(5): 117099.
[26] Song Q Z, Zha X D, Shi J J, et al. Development of TiO_2-doped MgO refractories with enhanced corrosion resistance for preparing high-purity nickel-based superalloys. Journal of Materials Research and Technology, 2025, 35: 402–415.
[27] Cui R, Gao M, Hu Z, et al. Interactions between TiAl alloys and yttria refractory material in casting process. Journal of Materials Processing Technology, 2010, 210(9): 1190–1196.
[28] Gao X Y, Zhang L, Qu X H, et al. Effect of interaction of refractories with Ni-based superalloy on inclusions during vacuum induction melting. International Journal of Minerals, Metallurgy and Materials, 2020, 27(11): 1551–1559.
[29] Mu H, Zhang T, Fruehan R J, et al. Reduction of CaO and MgO slag components by Al in liquid Fe. Metallurgical and Materials Transactions: B, 2018, 49: 1665–1674.
[30] Deng Z, Zhu M. Evolution mechanism of non-metallic inclusions in Al-killed alloyed steel during secondary refining process. ISIJ International, 2013, 53(3): 450–458.
[31] Jiang M, Wang X H, Wang W J, et al. Control of non-metallic inclusions by slag-metal reactions for high strength alloying steels. Steel Research International, 2010, 81(9): 759–765.
[32] Luo S J, Su Y H F, Lu M J, et al. EBSD analysis of magnesium addition on inclusion formation in SS400 structural steel. Materials Characterization, 2013, 82: 103–112.
[33] Wang L, Zhang Y, Chen C, et al. Effect of Al and Ti addition on the characteristics of oxide inclusions in Ni-based superalloy. Metallurgical Research & Technology, 2023, 120(2): 219.
[34] Gao R, Li L, Chen C, et al. Formation and aggregation behavior of inclusions in Ni-based alloys with different Mg contents. Journal of Materials Research and Technology, 2023, 26: 5252–5263.